Journal of Biomedical Optics 9(3), 618–623 (May/June 2004)

Dual modality instrument for simultaneous optical coherence tomography imaging and fluorescence spectroscopy

Jennifer Kehlet Barton
University of Arizona
Electrical & Computer Engineering Department
Division of Biomedical Engineering
1501 N Campbell, PO Box 245084
Tucson, Arizona 85724
and
University of Arizona
Optical Sciences Center
1230 East Speedway Boulevard
Tucson, Arizona 85721-0104
E-mail: barton@u.arizona.edu

Francisco Guzman
Alexandre Tumlinson
University of Arizona
Optical Sciences Center
1230 East Speedway Boulevard
Tucson, Arizona 85721-0104

Abstract. We develop a dual-modality device that combines the anatomical imaging capabilities of optical coherence tomography (OCT) with the functional capabilities of laser-induced fluorescence (LIF) spectroscopy. OCT provides cross-sectional images of tissue structure to a depth of up to 2 mm with approximately 10-μm resolution. LIF spectroscopy provides histochemical information in the form of emission spectra from a given tissue location. The OCT subsystem utilizes a superluminescent diode with a center wavelength of 1300 nm, whereas a helium cadmium laser provides the LIF excitation source at wavelengths of 325 and 442 nm. Preliminary data are obtained on eight postmortem aorta samples, each 10 mm in length. OCT images and LIF spectra give complementary information from normal and atherosclerotic portions of aorta wall. OCT images show structures such as intima, media, internal elastic lamina, and fibrotic regions. Emission spectra ratios of 520/490 (325-nm excitation) and 595/635 (442-nm excitation) could be used to identify normal and plaque regions with 97 and 91% correct classification rates, respectively. With miniaturization of the delivery probe and improvements in system speed, this dual-modality device could provide a valuable tool for identification and characterization of atherosclerotic plaques. [DOI: 10.1117/1.1695564]

Keywords: aorta; atherosclerosis; laser-induced fluorescence; multimodality; plaque.

Paper 03002 received Jan. 10, 2003; revised manuscript received Aug. 29, 2003; accepted for publication Sep. 4, 2003.

1 Introduction

Laser-induced fluorescence (LIF) techniques have been utilized for many years to discriminate between regions of abnormal and normal tissues. Differences in the autofluorescence emission spectra of healthy artery and atherosclerotic plaque have been documented by several researchers.[1–8] The feasibility of a real-time LIF system that can accurately discriminate between normal and atherosclerotic tissue in a blood-filled environment in patients has been demonstrated,[6] opening the possibility of using LIF to control laser angioplasty. Because LIF is sensitive to the chemical composition of the tissue under interrogation, LIF can also be used to determine the type of atherosclerotic lesion, including fibrous, fatty, and calcified.[4,5,8] Classification of lesion type has been successful using a range of excitation wavelengths from the UV to the blue. However, one study investigated wavelengths between 270 and 470 nm and concluded that optimum classification performance was achieved at excitation wavelengths between 314 and 334 nm, except for hard calcified plaques, which were more accurately classified with wavelengths longer[8] than 380 nm.

Optical coherence tomography (OCT) uses backscattered near-IR light to produce cross-sectional images of tissue.[9] A resolution of about 10 μ m is achieved with imaging depth of up to 2 mm in many tissues. OCT shows promise in distinguishing normal from diseased regions of several types of tissue, including bladder[10] and GI tract.[10,11] OCT has recently been utilized to locate and determine characteristics of atherosclerotic plaques *in vitro*[12–14] and *in vivo*.[15] *In vitro* studies have shown that aortic plaque structures such as lipid pools, calcifications, and fissures were visible in OCT images. *In vivo*, coronary fibrous and lipid-rich plaques were seen, as were microcalcifications and intimal hyperplasia. OCT was also shown to be superior to high-frequency intravascular ultrasound in resolution of plaque structural detail. However, in normal artery and plaque, penetration depth is limited to approximately 0.5 to 1.0 mm. These studies indicate that OCT shows promise for identifying features of coronary plaques at risk of rupture.

Since the data provided by LIF and OCT are distinct and complimentary, with LIF providing information about biochemical composition and OCT information about plaque boundaries, structure, and thickness, the combination of the two modalities may enable a higher sensitivity and specificity to a disease state than either modality alone. We built a dual-

Address all correspondence to Jennifer Kehlet Barton, Electrical & Computer Engineering Department, University of Arizona, 1501 North Campbell, PO Box 245084, Tucson, Arizona 85724. E-mail: barton@u.arizona.edu

1083-3668/2004/$15.00 © 2004 SPIE

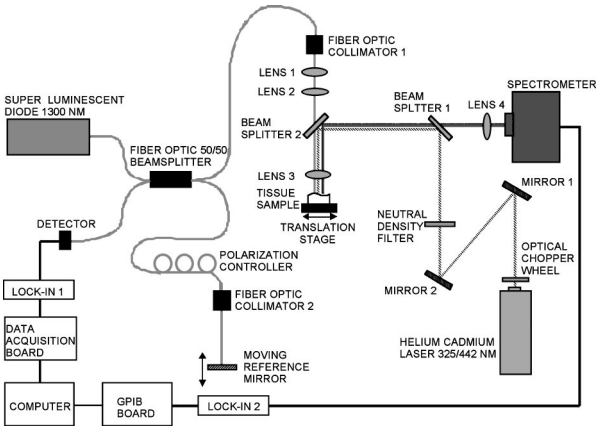

Fig. 1 Block diagram of the combined OCT-LIF system. The light gray, dashed, and dark gray lines show the paths of the OCT, excitation, and emission light, respectively.

purpose instrument that produces both high-resolution OCT images and fluorescence spectra. In this paper, we describe our instruments for obtaining simultaneous LIF spectra and OCT images, and present preliminary results obtained from autopsy aorta specimens.

2 Materials and Methods

2.1 *Dual-Modality Instrument*

A diagram of the experimental setup is shown in Fig. 1. The paths of the various light beams are indicated in the figure. The light gray line symbolizes the IR OCT light. The dashed line represents the laser excitation light, and the dark gray line signifies the path of the emitted fluorescence. As we can see, the optical paths of the OCT and LIF subsystems were distinct until they were combined in the sample arm, and analog processing electronics for the subsystems were distinct but controlled by a central computer.

2.2 *OCT Subsystem*

The OCT subsystem was similar to one described earlier.[16] The source was a 1300-nm-center-wavelength superluminescent diode (Superlum 561, Moscow, Russia) with a bandwidth of 49 nm, which gave a coherence length (and by definition axial resolution) of approximately 16 μm in air or 11 μm in tissue, assuming an average tissue index of refraction of 1.4. This source was combined with a 635-nm laser diode, which served as an aiming beam, and coupled into the source arm of a fiber Michelson interferometer. Because the speed of the overall device was limited by the scanning-grating spectrometer, a simple, slow galvanometer-mounted retroreflector was used in the OCT reference arm to provide 2 mm of pathlength modulation at 14 a-scans/s. The sample arm optics of the OCT subsystem are described subsequently. Light returning from the sample and the reference arm reentered the fiber interferometer and interfered when the pathlengths were matched to within a coherence length of the source. A photodetector was placed in the detection arm of the interferometer. The resulting signal was demodulated with a lock-in amplifier set to the heterodyne beat frequency of the moving reference mirror, approximately 98 kHz, and the demodulated signal was digitized with a data acquisition board. Incident power on the tissue was approximately 400 μW and the system had a dynamic range of 104 dB.

2.3 *LIF Spectroscopy Subsystem*

The LIF subsystem used as an excitation source a helium:cadmium (He:Cd) laser (Kimmon Electric, Englewood, Colorado), operating at 325 nm (15 mW) and 442 nm (72 mW). The laser beam was optically chopped at a frequency of 150 Hz to reduce noise and mitigate the effect of room lights. Two steering mirrors directed the path of the laser light, and a neutral density filter was used to reduce laser power on the sample. The laser light was reflected off a dichroic beamsplitter with a high reflectivity at the laser wavelength of choice and a high transmission at wavelengths slightly longer. Specifically, for 325-nm excitation the characteristics were 95% reflection at 325 nm and transmission of 5% at 340 nm, 80% at 360 nm and greater than 90% at 375 to 700 nm (350 DCLP, Chroma Technology Corporation, Brattleboro, Vermont). For use with 442-nm excitation, the beamsplitter had 98% reflection at 442 nm, transmission is greater than 90% from 470 to 600 nm and greater than 80% from 600 to 700 nm (460 DCLP, Chroma Technology Corporation). Light emitted from the sample and transmitted through the beamsplitter was focused into a scanning-grating spectrometer (Triax 180, Jobin Yvon, Edison, New Jersey). The emission light was detected by a photomultiplier tube (PMT) (H6780-04, Hamamatsu, Bridgewater, New Jersey). The output of the PMT was demodulated by a lock-in amplifier. A general purpose interface bus (GPIB) card controlled transfer of measured values from the amplifier to the computer. This same card was also used to control the spectrometer.

2.4 *Combined Sample Arm Optics*

The sample arm optics were designed so that the OCT and LIF excitation beams were coaligned on the sample. The optics were required to work over the wide wavelength range of 325 to 1325 nm. For the OCT subsystem, a long depth of focus and a spot size comparable to the source coherence length were desired. For the LIF subsystem, a larger spot size was desirable to avoid too high an irradiance (in watts per centimeter squared) and possible damage to the sample. The collection efficiency of the emission light was required to be made as large as possible. Finally, for ease of sample positioning it was desired that there be a large spacing between the final element and the tissue sample. The sample was mounted on a lateral translation stage to enable 2-D OCT images (b-scans) and multiple sites for LIF spectroscopy, so no steering optics were necessary in the sample arm design.

The design shown in Fig. 1 acceptably met all these criteria. Lens 3 was a calcium-fluoride (CaFl) lens used to focus both the laser excitation and OCT light onto the sample, and to collect the emission light. Uncoated CaFl provided transmission above 90% from 300 to 1500 nm. It was water soluble, but this limitation was not important in our setup. A 2 in. focal length on this lens enabled a reasonable working distance. Lenses 1 and 2 function as a beam-expanding telescope. The 9-μm fiber core diameter was reimaged twice for a net magnification of 1.2, creating an in-air spot size of 11 μm

at the sample plane (each lens was used at infinite conjugates, focal lengths: collimator = 11 mm; lens 1 = 25 mm; lens 2 = 100 mm; lens 3 = 50 mm).

The dichroic beamsplitter between lenses 2 and 3 combined the light from the LIF and OCT systems. The cold mirror (35-6923, Coherent, Santa Clara, California) had a transmission above 90% for near-IR light and a reflection above 90% for UV and visible light. The He-Cd laser had a 1.52 mm $1/e^2$ diameter so the waist diameter near the sample was 14 μm. Due to chromatic aberration in the final lens, the distance to the focus for 325-nm light was actually 2.7 mm less than for the 1300-nm OCT beam. Gaussian beam calculation shows that the 325-nm beam expanded to 70 μm before reaching the tissue surface. The numerical aperture of the emission light collection system was limited by lens 3 and was 0.18.

2.5 *Software and Image Acquisition*

LabVIEW software (National Instruments, Austin, Texas) was used to synchronize OCT reference arm movement and for data acquisition, sample lateral translation, spectrometer control, and LIF spectra measurement. The software also processed and displayed the images. The background (system response with laser shutter closed) was indistinguishable from noise and insensitive to room lights. System response measured with a calibrated light source (LS-1-CAL, Ocean Optics, Dunedin, Florida) was divided through all measured spectra.

Because LIF spectra required approximately 120 s to acquire, imaging and spectra acquisition were staggered. An LIF spectra was obtained at the beginning of the area of interest, then the sample stage was translated a designated distance while a partial OCT image was obtained. Then, another spectra was obtained after which OCT imaging continued. This sequence was repeated until the desired length image was obtained (6 to 10 mm), and ended with a spectra acquisition. To avoid any geometrical effects, the sample was manually translated at the beginning of every spectra measurement to be the same distance from lens 3.

2.6 *Tissue Samples*

Aorta samples were obtained postmortem from the University Medical Center morgue, frozen, then thawed prior to measurement. The subjects were both male and female, ranging in age 56 to 89. To determine the effect of freezing on the samples, one sample was examined both fresh (< 48 h postmortem) and after freezing for 14 days and thawing. Grossly, all samples had slightly raised lesions on a smooth flat background. Imaging and fluorescence measurements included both lesion and flat portions of the sample. During imaging, the tissue was kept moist with isotonic saline solution. After images and spectra were obtained, the samples were placed in an alcohol-based fixative, processed by standard histological methods, sectioned along the measured plane, and stained with hematoxylin and eosin.

3 Results

OCT and fluorescence spectra were successfully obtained from eight aorta samples. Histological examination showed that the slightly raised areas on the samples were fibrotic/fatty plaques, and that the smooth flat portions of the aorta were normal with mild intimal hyperplasia consistent with the age of the donors. No calcified regions were identified. All spectra locations were placed into three categories: normal, plaque, or transition, the latter defined as locations within 0.5 mm of the edge of a raised region, so emission could be collected from both normal aorta and plaque.

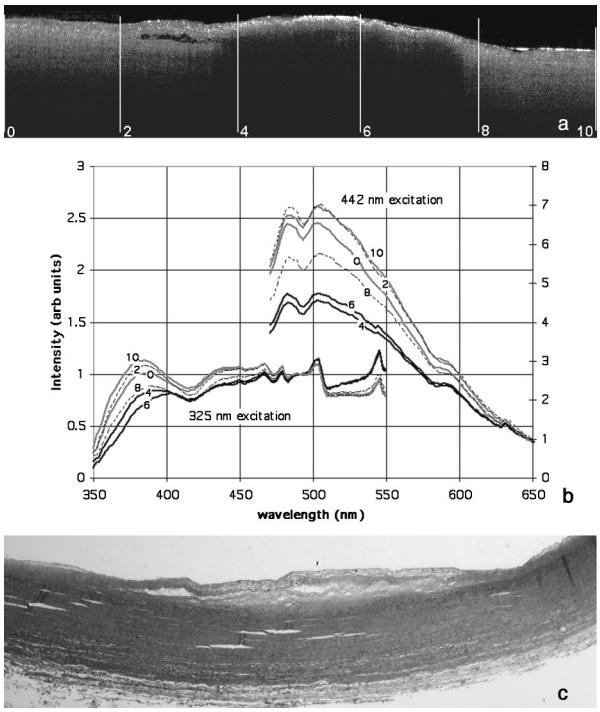

Fig. 2 (a) OCT, (b) fluorescence spectra, and (c) histology from an example sample of abdominal aorta. A slightly raised plaque is seen in the center of the OCT and histology images. At the shorter emission wavelengths, spectra from the plaque regions have lower relative intensity compared to normal regions for both excitation wavelengths.

For one example aorta sample, the following are displayed: OCT image, fluorescence emission spectra, and corresponding histology. Figure 2(a) shows the OCT image, which is 1.4 mm in depth and 10 mm in lateral dimension. The plaque area appears as a highly backscattering layer over a signal-poor region, and a dissection is seen between the 2- and 4-mm locations. Fluorescence spectra were obtained every 2 mm along the length of the scan (for a total of six spectra); locations are marked on the OCT image with white lines. In Fig. 2(b), fluorescence spectra are shown for emission wavelengths of 350 to 550 nm (325-nm excitation) and 467 to 650 nm (442-nm excitation). Emission spectra for 325-nm excitation were normalized to intensity at 490 nm, whereas spectra for 442-nm excitation were normalized to intensity at 635 nm. Normalization wavelengths were determined empirically to enable the best comparison of spectral shape. All raw spectra were corrected for the system response. Numbers next to the curves in Fig. 2(b) give corresponding locations on the OCT image. Gray, black, and dashed curves are spectra from areas identified as normal, plaque, and transition, respectively, in the histology image [Fig. 2(c)].

For both excitation wavelengths, we see that the ratio of the intensity of plaque to normal regions at the shorter emis-

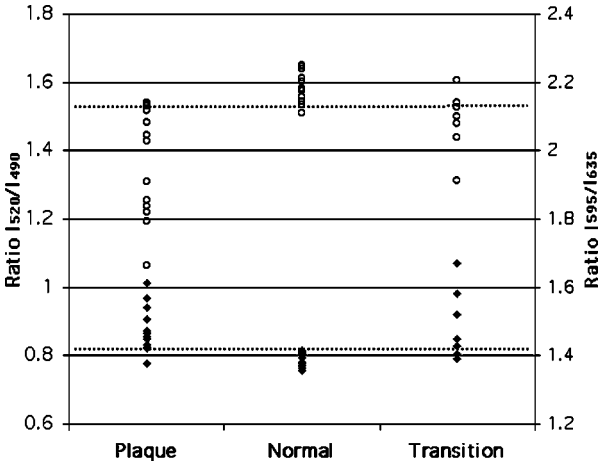

Fig. 3 Summary of all spectra. The ratio of intensities at 520 to 490 nm (for 325-nm excitation—represented as closed diamonds) and 595 to 635 nm (for 442-nm excitation—shown as open circles) are given for plaque, normal, and transition (edge of plaque) regions.

sion wavelengths is lower than at the longer emission wavelengths. Transition spectra are variable. A pronounced dip in the spectra at 420 nm (325-nm excitation) is attributed to hemoglobin absorption, as are less obvious decreases at 540 and 580 nm (442-nm excitation). Sharp features in the emission spectra (i.e., bumps at wavelengths longer than 450 nm for 325-nm excitation, and a dip at 485 nm and bump at 595 nm for 442-nm excitation) appear to be failures of the calibration routine, perhaps caused by fluorescence of the dichroic beamsplitters. Raw intensities were low at these wavelengths.

All emission spectra (35 at each excitation wavelength) are summarized in Fig. 3. In this figure the ratio of intensities at 520 to 490 nm (for 325-nm excitation—represented as closed diamonds) or 595 to 635 nm (for 442-nm excitation—shown as open circles) are plotted. The ratios for normal tissues are seen to be fairly consistent from sample to sample, whereas the ratios for plaque regions have more variability, perhaps reflecting the biochemical diversity of various plaques. Transition spectra are highly variable as well. If $I_{530}/I_{490}<0.82$ or $I_{595}/I_{635}>1.13$ is considered to be normal, regions of plaque

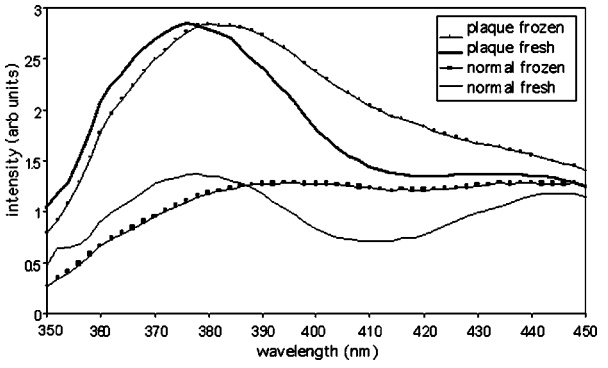

Fig. 4 Spectra (325-nm excitation) taken from the same two locations (one normal, one plaque) before and after freezing a sample for 14 days. Strong hemoglobin absorption at 420 nm apparent in the fresh spectra is nearly absent in the frozen spectra.

and normal tissue are correctly classified 97 and 91% of the time when 325- and 442-nm excitation wavelengths are used, respectively.

Figure 4 shows emission spectra over the range 350 to 450 nm (325-nm excitation) for the same two positions—one normal and one plaque—on a sample both fresh ($<$48 h postmortem) and frozen then thawed. The plaque fresh and frozen spectra are normalized to peak value. The normal spectra are normalized to their respective plaque spectra at 490 nm. The fresh spectra show a pronounced dip at 410 to 420 nm that is not present in the frozen spectra.

4 Discussion

We reported a unique system capable of acquiring OCT images and fluorescence emission spectra. A fluorescence-image-guided OCT probe has previously been presented,[17] where a wide-field-of-view fluorescence image is used to identify candidate tissue regions for OCT imaging. The reported system has the advantage that large areas can be scanned quickly and only regions that have abnormal fluorescence in an integrated wavelength range are investigated in detail with OCT. In contrast, our system uses LIF and OCT as complementary technologies for characterizing the same tissue location, and acquires wavelength-resolved fluorescence emission data. Our system, which uses a separate light source for OCT imaging and fluorescence spectroscopy, is fundamentally different from spectroscopic OCT.[18] The latter technique examines the spectrum of the backscattered light, from which absorption properties of the tissue can be inferred. In another instrument, combined optical coherence microscopy (OCM) and two-photon-excited fluorescence microscopy has been demonstrated.[19] This system provides information on both the tissue morphology and biochemistry using a single femtosecond-pulse laser to generate both signals. Since both OCM and two-photon spectroscopy rely on high-numerical-aperture focusing optics and careful objective-sample spacing, this system may be less easily adapted for endoscopic applications than the dual-modality system presented here. It may be possible to perform OCT and fluorescence spectroscopy with a single light source, if a broadband source with sufficiently short center wavelength to excite endogenous or exogenous fluorophores was used. A recently reported[20] visible OCT could meet this criterion. In this case, beamsplitter 1 would be unnecessary and beamsplitter 2 would need to be carefully chosen to reflect wavelengths longer than those present in any significant amount in the source.

The OCT images showed features similar to those seen by previous researchers,[12–15] such as layered structures attributed to the intima, internal elastic lamina and media in normal aorta, and dissections, small lipid pools (low backscattering), and fibrotic areas (higher backscattering) in the plaque regions. The LIF trends seen in this study agree with previously published research. For instance, Lucas et al.[4] found that coronary artery atherosclerotic lesions had an increased normalized fluorescence intensity at longer wavelengths: $>$500 nm when excited with 325 nm. Andersson-Engels et al.[3] data also had a higher ratio of emission intensity (520 to 490 nm) for aortic plaque, in this case for excitation at 337 nm. In atherosclerotic aorta, main fluorophores are collagen, elastin, and ceroid, and the emission spectrum is strongly in-

fluenced by hemoglobin absorption. Intima is mainly collagen, whereas the media is mainly elastin. Both collagen and elastin have similar emission spectra (broad peak from approximately 400 to 500 nm at 325-nm excitation, and 470 to 570 with 442-nm excitation), but elastin has a greater efficiency. Intimal thickening and thus attenuation of the media elastin signature may be responsible for the relative emission intensity decrease at shorter wavelengths.[21]

It appears that both excitation wavelengths of 325 and 442 nm are capable of differentiating normal from plaque regions, and can achieve similar correct classification rates (Fig. 3). A significant increase in data acquisition speed could be achieved by eliminating one excitation wavelength. However, the lesions examined in this study were all very similar (slightly raised fibrotic/fatty plaques), and it may be that with a more heterogeneous sample set a combination of wavelengths would be useful for discrimination between types of lesions.

The comparison of LIF spectra obtained from the fresh and frozen/thawed samples (Fig. 4) illustrates the importance of sample handing on the results obtained. LIF spectra from aorta, with fluorescence from structural proteins and ceroid, are less sensitive to tissue viability than are spectra from other tissues such as colon or cervix where measuring the metabolic state of the tissue is a major goal. However, contrary to previous reports,[2,5] we found that the freshness of the aorta tissue affected at least the hemoglobin absorption around 420 nm. Since the tissue was not washed during the freezing and thawing procedure, and thus it is expected that a minimal amount of blood was lost during the procedure, it is possible that the some of the hemoglobin changed form (for instance from oxyhemoglobin to deoxy- or methemoglobin) form during freezing. This change in hemoglobin absorption complicates spectra interpretation. What appears to be a red shift in the emission spectra of the frozen/thawed sample is most likely only an artifact of the normalization process and reduced contribution of hemoglobin absorption around 420 nm.

From these data, an appreciation for the heterogeneities of the tissue was obtained. The OCT images showed that the structure of a plaque often varied across its extent, and in these cases the LIF spectra also changed from location to location on the plaque. Therefore, an OCT image of a complicated plaque may help explain a confusing LIF spectra. A much more extensive study is necessary before a determination could be made as to whether the two modalities in combination can provide a better classification of disease state than can either modality alone. However, even if no improvement in classification is seen, a dual-modality instrument is useful for other reasons. OCT has the capability to measure quantities such as layer thicknesses and distance from the sample arm optics to the tissue surface. The former quantity is important in developing models that attempt to explain fluorescence spectra based on fluorophore concentrations as a function of depth.[22] The latter quantity can be used to correct for differences in the detected power with changes in optics-tissue separation. A compensation algorithm has been published, using ultrasound a-mode to provide separation information.[23] In our system, this method can be used to eliminate manual repositioning of the sample at LIF measurement points. OCT images clearly delineated the mild (slightly raised) plaques imaged in this study, and the excellent correct classification rate using fluorescence spectra suggest that this instrument has the potential to detect the early stages of plaque development. However, additional studies with a greater number and diversity of atherosclerotic plaques are necessary to make a full determination of system utility.

For use *in vivo*, catheter-based sample arm optics and system acquisition speed improvements are necessary. We are currently building a miniature dual-modality endoscope.[24] Intravascular use necessitates some means of minimizing the blood between the optics and the tissue, for instance by saline flushing[15] or positioning wire.[25] Ongoing work also includes decreasing emission spectra measurement time by use of a cooled CCD in place of the scanning grating/photomultiplier system, and investigation of additional tissues. Preliminary experiments in mouse colon have show promise for identification of early adenomas.

Acknowledgments

The authors appreciate the assistance of Ms. Faith Rice and Dr. Stuart Williams in preparation and interpretation of histology, and University Medical Center pathology for the samples. This work was supported in part by grants from the National Science Foundation (9978820) and the National Institutes of Health (CA83148). Tissue was obtained from the National Disease Research Interchange.

References

1. C. C. Hoyt, R. R. Kortum, B. Costello, B. A. Sacks, C. Kittrell, N. B. Ratliff, and M. S. Feld, ''Remote biomedical spectroscopic imaging of human artery wall,'' *Lasers Surg. Med.* **8**, 1–9 (1988).
2. M. Satori, D. Weilbaecher, G. L. Valderrama, S. Kubodera, R. C. Chin, M. J. Berry, F. K. Tittel, R. Sauerbrey, and P. D. Henry, ''Laser-induced autofluorescence of human arteries,'' *Circ. Res.* **63**, 1053–1059 (1988).
3. S. Andersson-Engles, J. Johnansson, U. Stenram, K. Svanberg, and S. Svanberg, ''Malignant tumor and atherosclerotic plaque diagnosis using laser-induced fluorescence,'' *IEEE J. Quantum Electron.* **26**, 2207–2217 (1990).
4. A. Lucas, M. J. Radosavljevic, E. Lu, and E. J. Gaffney, ''Characterization of human coronary artery atherosclerotic plaque fluorescence emission,'' *Can. J. Cardiol.* **6**, 219–228 (1990).
5. J. J. Baraga, R. P. Rava, P. Taroni, C. Kittrell, M. Fitmaurice, and M. S. Feld, ''Laser induced fluorescence spetroscopy of normal and atherosclerotic human aorta using 306–310 excitation,'' *Lasers Surg. Med.* **10**, 245–261 (1990).
6. A. L. Bartorelli, M. B. Leon, Y. Almagor, L. G. Prevosti, J. A. Swain, C. L. McIntosh, R. F. Neville, M. D. House, and R. F. Bonner, ''In vivo human atherosclerotic plaque recognition by laser-excited fluorescence spectroscopy,'' *J. Am. Coll. Cardiol.* **17**, 160B–168B (1991).
7. F. Bosshart, U. Utzinger, O. M. Hess, J. Wyser, A. Muller, J. Schneider, P. Niederer, M. Anlider, and H. P. Krayenbuehl, ''Fluorescence spectroscopy for identification of atherosclerotic tissue,'' *Cardiovasc. Res.* **26**, 620–625 (1992).
8. A. L. Alexander, C. M. Connor Davenport, and A. F. Gmitro, ''Comparison of illumination wavelengths for detection of atherosclerosis by optical fluorescence spectroscopy,'' *Opt. Eng.* **33**, 167–174 (1994).
9. D. Huang, E. A. Swanson, C. P. Lin, J. S. Schuman, W. G. Stinson, W. Chang, M. R. Hee, T. Flotte, K. Gregory, C. A. Puliafito, and J. G. Fujimoto, ''Optical coherence tomography,'' *Science* **254**, 1178–1181 (1991).
10. A. M. Sergeev, V. M. Gelikonov, G. V. Gelikonov, F. I. Feldchtein, R. V. Kuranov, N. D. Gladkova, N. M. Shakhova, L. B. Snopova, A. V. Shakhov, I. A. Kuznetzova, A. N. Denisendo, V. V. Pochinko, Y. P. Chumakov, and O. S. Streltzova, ''*In vivo* endoscopic OCT imaging of precancer and cancer states of human mucosa,'' *Opt. Express* **1**, 432–440 (1997).

11. A. Das, M. V. Sivak, Jr, A. Chak, R. C. Wong, V. Westphal, A. M. Rollins, J. Willis, G. Isenberg, and J. A. Izatt, ''High-resolution endoscopic imaging of the GI tract: a comparative study of optical coherence tomography versus high-frequency catheter probe EUS,'' *Gastrointest. Endosc.* **54**, 219–224 (2001).
12. M. E. Brezinski, G. J. Tearney, B. E. Bouma, J. A. Izatt, M. R. Hee, E. A. Swanson, J. F. Southern, and J. G. Fujimoto, ''Optical coherence tomography for optical biopsy: properties and demonstration of vascular pathology,'' *Circulation* **93**, 1206–1213 (1996).
13. M. E. Brezinski, G. J. Tearney, N. J. Weissman, S. A. Boppart, B. E. Bouma, M. R. Hee, A. E. Weyman, E. A. Swanson, J. F. Southern, and J. G. Fujimoto, ''Assessing atherosclerotic plaque morphology: comparison of optical coherence tomography and high frequency ultrasound,'' *Heart* **77**, 397–403 (1997).
14. H. Yabushita, B. E. Bouma, S. L. Houser, H. T. Aretz, I. Jang, K. H. Schlendorf, C. R. Kauffman, M. Shishkov, D. Kang, E. F. Halpern, and G. J. Tearney, ''Characterization of human atherosclerosis by optical coherence tomography,'' *Circulation* **106**, 1640–1645 (2002).
15. I. Jang, B. E. Bouma, D. Kang, S. Park, S. Park, K. B. Seung, K. Choi, M. Shishkov, K. Schlendorf, E. Pomerantsev, S. Houser, R. Aretz, and G. J. Tearney, ''Visualization of coronary atherosclerotic plaques in patients using optical coherence tomography: comparison with intravascular ultrasound,'' *J. Am. Coll. Cardiol.* **39**, 604–609 (2002).
16. J. A. Izatt, M. D. Kulkarni, S. Yazdanfar, J. K. Barton, and A. J. Welch, ''In vivo bidirectional color Doppler flow imaging of picoliter blood volumes using optical coherence tomography,'' *Opt. Lett.* **22**, 1439–1441 (1997).
17. R. J. McNichols, A. Gowda, B. A. Bell, R. M. Johnigan, K. H. Calhoun, and M. Motamedi, ''Development of an endoscopic fluorescence image-guided OCT probe for oral cancer detection,'' *Proc. SPIE* **4254**, 23–30 (2001).
18. U. Morgner, W. Drexler, F. X. Kartner, X. D. Li, C. Pitris, E. P. Ippen, and J. G. Fujimoto, ''Spectroscopic optical coherence tomography,'' *Opt. Lett.* **25**, 111–113 (2000).
19. E. Beaurepaire, L. Moreaux, F. Amblard, and J. Mertz, ''Combined scanning optical coherence and two-photon-excited fluorescence spectroscopy,'' *Opt. Lett.* **24**, 969–971 (1999).
20. B. Poyazay, A. Apolonski, A. Unterhuber, B. Hermann, K. Bizheva, H. Saltmann, P. Russell, F. Krausz, A. Fercher, and W. Drexler, ''Visible light optical coherence tomography,'' *Proc. SPIE* **4619**, 90–94 (2002).
21. R. Richards-Kortum, R. P. Rava, M. Fitzmaurice, L. L. Tong, N. B. Ratliff, J. R. Kramer, and M. S. Feld, ''A one-layer model of laser-induced fluorescence for diagnosis of disease in human tissue: applications to atherosclerosis,'' *IEEE Trans. Biomed. Eng.* **36**, 1222–1232 (1989).
22. A. J. Welch, C. Gardner, R. R. Richards-Kortum, E. Chan, G. Criswell, J. Pfefer, and S. Warren, ''Propagation of fluorescent light,'' *Lasers Surg. Med.* **21**, 166–178 (1997).
23. S. Warren, K. Pope, Y. Yazdi, A. J. Welch, S. Thomsen, A. J. Johnston, M. J. Davis, and R. Richards-Kortum, ''Combined ultrasound and fluorescence spectroscopy for physico-chemical imaging of atherosclerosis,'' *IEEE Trans. Biomed. Eng.* **42**, 121–132 (1995).
24. A. Tumlinson, L. Hariri, and J. K. Barton, ''Miniature endoscope for a combined OCT-LIF system,'' *Proc. SPIE* **4956**, 129–138 (2003).
25. J. K. Barton, D. B. DalPonte, S. K. Williams, B. Ford, and M. R. Descour, ''Imaging vascular implants with optical coherence tomography,'' *Proc. SPIE* **3915**, 229–236 (2000).